Master's Thesis of Engineering

Swarm Control of Shape Memory Alloy based Microrobots

형상기억합금을 사용한 마이크로 로봇의 군집제어

February 2020

Graduate School of Engineering
Seoul National University
Department of Mechanical & Aerospace Engineering
Yu, Chak Yuk

Swarm Control of Shape Memory Alloy based Microrobots

Academic advisor Prof. Ahn, Sung-Hoon

Submitting a master's thesis of Public Administration

October 2019

Graduate School of Engineering
Seoul National University
Department of Mechanical & Aerospace Engineering

Yu, Chak Yuk

Confirming the master's thesis written by
Yu, Chak Yuk
December 2019

Chair _____(Seal)
Vice Chair _____(Seal)
Examiner _____(Seal)

Abstract

The development of microrobots brings many great potential values in the microscale world such as to be implemented with small-scale applications for miniaturized operations in improving the existing technology of health care and providing more bioengineering solutions. In this study, a microrobot made of shape memory alloy (SMA) fabricated under focused ion beam (FIB) is introduced, trained to have a two-way shape memory effect (TWSME), which can be successfully driven by laser scanning exhibiting a crawling motion with reaching a maximum speed up to 150.1 μm s^{-1} with a short scan size (1 mm). A basic and simple swarm control methodology has been constructed successfully to manipulate multiple SMA microrobots to perform different actuation motions following the designated laser pathway. The direction of laser scanning can control the direction of the actuation of the robot, high maneuverability of controlling the microrobots can be realized by assigning the robots to reach the targeted destinations. It is proposed that the functionality can be broadened with implementing with the ability to transport and release substances or to exhibit a punching motion.

Keyword : swarm, lasers, microrobots, shape memory alloys, smart materials

Student Number : 2018-27049

Table of Contents

List of Tables

List of Figures

Chapter 1. Introduction

1.1. The world of microscale actuation

Actuation in microscale has been widely studied with developing a wide range of applications such as biomedical devices, microsensors and microfluidic devices for microelectromechanical system (MEMs) [1]. The reason why makes the microscale actuation important is to implement with small-scale application for miniaturized operations in improving the existing technology of health care and providing more bioengineering solutions [2].

One of the highest potential scientific application would be the development of microrobots. In order to replace the role of the existing tethered and milli scale medical devices such as flexible endoscopes and catheters, mobile microrobots could access more complex and small regions of the human body such as blood capillaries, spinal cord and even brain, which have not been possible to access currently with existing technologies for high-resolution in situ and in vivo manipulations [1, 3-4].

To a smaller and narrower cell culturing aspect, a microscale robot could help weave and construct a cell network when the size of the robots is similar to the human cell [5, 6]. Such that, Bio-MEMs devices are no longer limited to the traditional manufacturing methods such as lithography, micromachining and micro molding, with the aid from microrobots, a more

complex cell network or pattern can be illustrated with the specific designated control algorithm and the cooperation work from the robots, instead of two-dimensional space on a flat surface, a three-dimensional kinematics and dynamics can be achieved in the future.

Various propulsion technologies have been developed to power micro and nano robots. Advance strategies can be broadly divided into three categories: self-propulsion, external propulsion, and a hybrid strategy including both [7]. Self-propelled methods are typically based on local chemical reactions that occur on small mechanical surfaces where chemical energy is converted to kinetic energy [8-10]. This energy conversion leads to the movement of micro and nano robots. Alternatively, an external power source can be used to precisely control the locomotion of micro and nano robots. This approach is more desirable for biomedical applications that require precise positioning. These external sources of energy can be provided by magnetic fields, light, acoustic waves, electric fields, thermal energy, or combinations of these [11-13, 33-37]. A recent trend is to use the function of a motile microorganisms to combine with a stimulus-responsive building block such as a magnetic component so that it can be manipulated using an external power source [14, 15]. Table 1 summarizes and lists the characteristics including advantages and limitations of all types of small robots [7].

Table 1. Summarization of propulsion technologies of small-scale robots [7]

	Key features	Advantages	Limitations
Self-propulsion	Use chemical reactions to generate propulsion force	High speed; Low cost	Continuous fuel supply is needed for powering; Most of the fuels are toxic; Lack of directionality
External propulsion	External power provided by magnetic fields, light, acoustic fields, electric fields, etc., for actuation	Position precisely controlled; Good directionality	Special manipulating equipment is usually essential.
Hybrid actuation strategy	Combination of different actuation strategies, including self-powered strategies, externally powered strategies, and motile live cells or microorganisms	Relatively efficient in power output; Good control on directionality; Responsive to multiple stimuli	Live cells survive only under certain conditions; Difficult precise control

1.2. The role of Shape Memory Alloy

Various types of smart materials with unique characteristics such as shape memory alloys (SMAs), piezoelectric materials and magnetic materials have used for different specific actuation methodology to provide actuation power for micro/nanoscale actuators with different applications [16-19]. Among these materials, SMAs have strong advantages in term of power-to-weight ratio and mechanical properties (e.g. stress and strain, young modulus, etc.), as they can generate a large force within small volume [20-24].

Numerous studies have been carried out to demonstrate the usage of shape memory effect as actuation methodology in different scales [25-30]. However, most researches only focused on the application with bulky structure making it impractical to achieve actual implementation in daily life. In order to extend the uses of practical applications, investigation and improvement on geometries of shape memory alloy with providing actuation in more degree of freedom is necessary.

Shape memory alloy is a class of alloy material that an memorize a shape and undergo deformation with reverting back to original shape which can recover apparent permanent strains when they are heated above a certain temperature, which means it is an alloy that can remember its original shape and it can return to its pre-deformed shape when heated [29].

The reason why makes shape memory alloy different from other metal alloys is because of its shape memory effect (SME) providing the ability of restoring the original shape of a plastically deformed sample and pseudoplasticity as an elastic response to an applied stress without the need of any thermal activation. There are two phases of shape memory alloy, one is martensite phase, and one is austenite phase. In martensite phase, it is the normal state of shape memory alloy before heated in which the alloy is weaker but more ductile compared to its high temperature state in austenite phase.

For the shape memory effect, it is basically done by the martensitic transformation. The transformation from one structure to the other structure does not occur by diffusion of atoms, but rather by shear lattice distortion on its structure. Two mechanisms are needed to transform between austenite and martensite phase. One is to apply high stress which can change shape memory alloy to martensite phase; and the other one is to heat SMA to change it to austenite phase. Briefly, material in these phases can be loaded and undergo significant plastic deformation and return to original shape through heating (see Figure 1) [29, 31-32]. Compared to other smart material such as piezoelectric materials and magnetic materials, due to the high power to weight ratio of shape memory alloy, it can provide larger actuation force with higher mechanical performances. And the shape

recovery can be observed even in micro-scale. The detailed mechanical performances of NiTi is stated in the following table.

Table 2. Material properties of NiTi used. (Dynalloy, Inc. (USA)) [29, 31]

Material Properties	Value
Density	6.45 g/cm^3
Melting point	1240-1310 °C
Specific heat	470-620 J/kg°C
Latent heat	24200 J/kg
Nickel Content	0.48
M_s temperature (transformation temperature)	90 °C
Thermal conductivity (austenite)	18 W/m°C
Thermal conductivity (martensite)	8.6 W/m°C
Coefficient of thermal expansion (austenite)	11×10^{-6} /°C
Coefficient of thermal expansion (martensite)	6.6×10^{-6} /°C
Elastic modulus (austenite)	75–83 GPa
Elastic modulus (martensite)	28–40 GPa
Yield strength (austenite)	195–690 MPa
Yield strength (martensite)	70–140 MPa
Ultimate tensile strength	750-960 MPa
Shape memory strain (Max.)	~8.0 %
Poisson's ratio	0.33

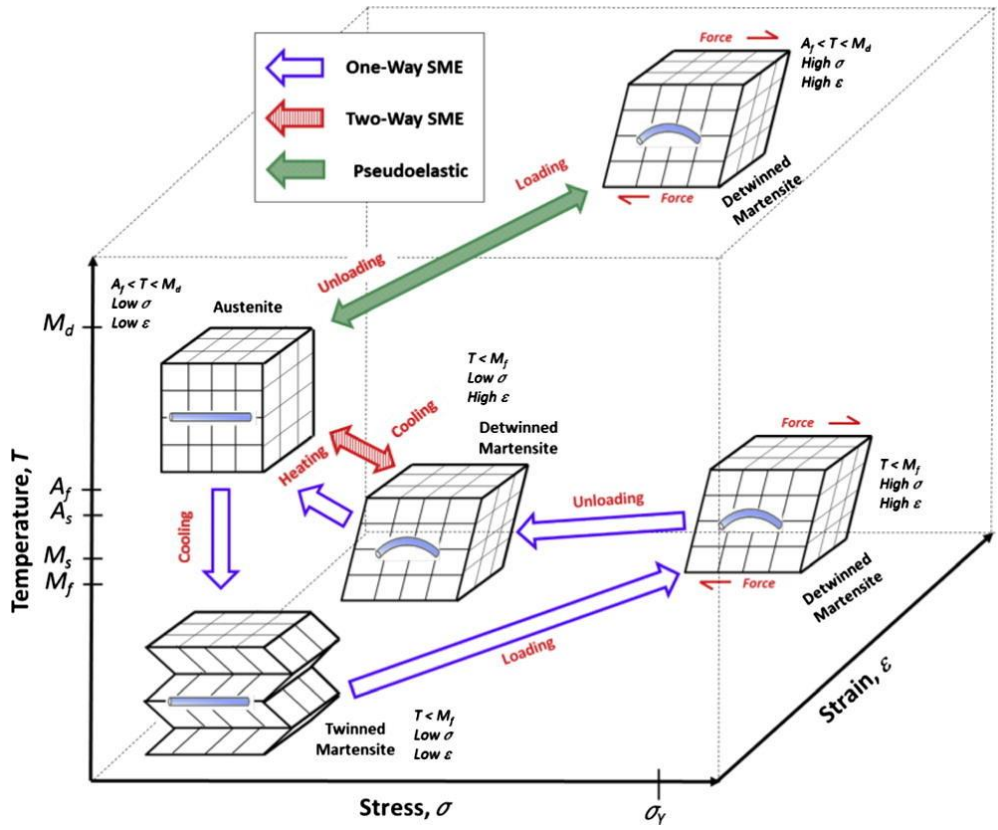

Figure 1. Phase transformation of SMA [29]

1.3. Literature Review

While, although the current hot topic on providing solutions for micro-actuation is to use magnetic materials as a strong magnetic field can penetrate the human body to detect and maneuver the microscale devices within the interior [33-37], a cumbersome operation system should be considered well in order to provide a constant and stable strong enough magnetic field supply with high controllability to provide a three-dimensional steering inside the body as the tissues of the human body as well as the air in between the coil and the patient may block or reduce the magnetic fields generated [1]. And the common manual faulty operation may easily lead to a serious problem.

For these reasons, numerous studies have been performed to determine how to apply shape memory effects to microscale actuation. Krulevitch et al. demonstrated the potential of NiTi as an actuating source for microscale actuators [17]. Gill et al. developed a thin-film NiTi micro wrapper; the arms of the micro wrapper flatten and curl up according to the temperature [38]. Ali et al. reported a spiral-coil shaped actuator which is controlled by external radio frequency magnetic field [39]. Takeuchi proposed a microelectrode with an SMA clipping structure [40]. Inspired by the human muscles' anatomy, many research groups have tried to mimic artificial muscles based on SME, however, most studies only focus on bulk muscle

being lack of investigating in skeletal muscles composed of the hundreds of muscle fibers, each 10–100 μm in diameter, providing high resolution and precision in muscular motion control [41].

However, relatively slow actuation speed and low strain range less than 10% is known as limitations of SMA [42]. From the previous work, an SMA based microscale actuators consist of diamond-shaped frame structures was developed [43] with successfully demonstrating a large elongation range compared with bulk SMA materials, with the aid of spring-like behavior under tensile deformation, in which the frequency can be up to 1600 Hz allowing high-speed actuation due to scale effect, which is more similar to the excitation mechanism of real muscles. To actuate and control the microscale SMA actuators, a laser-based control system was devised with investigation on force and response speed with varying the laser switching speed and irradiation energy.

On the other hand, the working condition of a microscale robot or any other devices used inside human body mostly consists of fluid-filled lumens and cavities as well as soft tissues. Microscale devices must be designed specifically to work in these environments, but the relative changes in the size, geometry, and the material properties of the environment within a given procedure present design challenges. In order to overcome different obstacles in the working environment, more degrees of freedom or smarter

mechanism is necessary for better maneuverability. Pawashe et al. performed a multiple magnetic microrobot control using electrostatic anchoring. Four independent square-turn electromagnetic coils were used to actuate two magnetic microrobots [44]. Although they showed successful multiple independent transitions of two microrobots, due to the electromagnetic arrangement, there is no possible collaboration between multiple robots. The functionality is still limited.

As the existing studies are all limited due to the fundamental engineering design and fabrication challenges, the value of practical usage is still blurred. Thus, in order to facilitate the maneuverability of the control methodology of actuating multiple microrobots at the same time, we proposed to use laser to transfer energy as the actuation power source for SMA microrobots which can be assumed as a reliable and stable mechanism except of its disability of transferring energy beyond obstacles.

An independent operation of a microrobot made of SMA was successfully demonstrated previously performing a crawling-like motion with a maximum speed of 10.0 μm s^{-1}, which is controlled by laser scanning [48]. During actuation, the motion of the robot is triggered by the shape memory effect and the propulsion induced by optothermal and optical trapping effects. However, due to the unstable manufacturing process and the challenges in the controllability, a swarm robotics is still being hindered.

Chapter 2. Research Objectives

In this study, microrobots made of shape memory alloy consisting of the diamond-shaped frame structure is developed and fabricated through Focused Ion Beam machine (FIB) with improved manufacturing process based on the previous work [48]. The maneuverability of the improved robots is demonstrated with the optimizing the actuation performance of microrobot.

The goal of this research is to develop a swarm control methodology to manipulate multiple SMA microrobots to perform different accurate and precise designated actuation motions such as linear motion, bending motion, rotation, and torsion, allowing more variability and diversifications on the solutions to implement microrobots with high steerability in order to overcome the existing challenges.

The functionality of microrobot is also considered through adding functional features on the robots like knife-shaped head, scissor-shaped head and gripper head, such that it can be proven that the microrobots are able to transport and deliver targeted objects to specific positions.

Chapter 3. Fabrication Process

3.1. Focused Ion Beam technique

Microfabrication technology is a broad term that encompasses literally hundreds of techniques in which three categories have been extensively used, photolithography, micromachining and soft lithography. Despite the enormous differences between microelectronics and biomedicine, the forces that have driven the trend toward miniaturization are similar in both fields from electronics to cells, and to fluids. Microfabrication techniques are beneficial to biomedical applications with providing small-scale benefit, high-throughput benefit and quantitative benefit [45].

A focused ion beam system (FIB) is a relatively new tool that has a high degree of analogy with a focused electron beam system such as a scanning electron microscope or a transmission electron microscope. In these systems the electron beam is directed towards the sample, and upon interaction it generates signals that are used to create high magnification images of the sample. As the beam is well controlled in size and position and the signals are strong enough to be detected without excessive noise, these kinds of tools are very powerful to analyze samples in detail over a wide range of magnifications.

Different from other scanning electron microscopy (SEM) and energy dispersive spectroscopy, a different particle is used to create the primary beam that interacts with the sample. Usually, gallium is commonly used as the source to be heated up to generate Ga+ ions continuously to be focused and formed into a beam through acceleration. As the name FIB indicates, ions are used instead of electrons compared to SEM.

While, FIB processing can be categorized as four basic functions, milling (sputtering and etching), deposition, implantation and imaging (see Figure 4) [46]. Unlike an electron microscope, FIB is inherently destructive to the specimen. When the high-energy gallium ions strike the sample, they will sputter atoms from the surface. Gallium atoms will also be implanted into the top few nanometers of the surface, and the surface will be made amorphous.

All fabrication processes were performed in the custom-manufactured FIB system described as Figure 5.

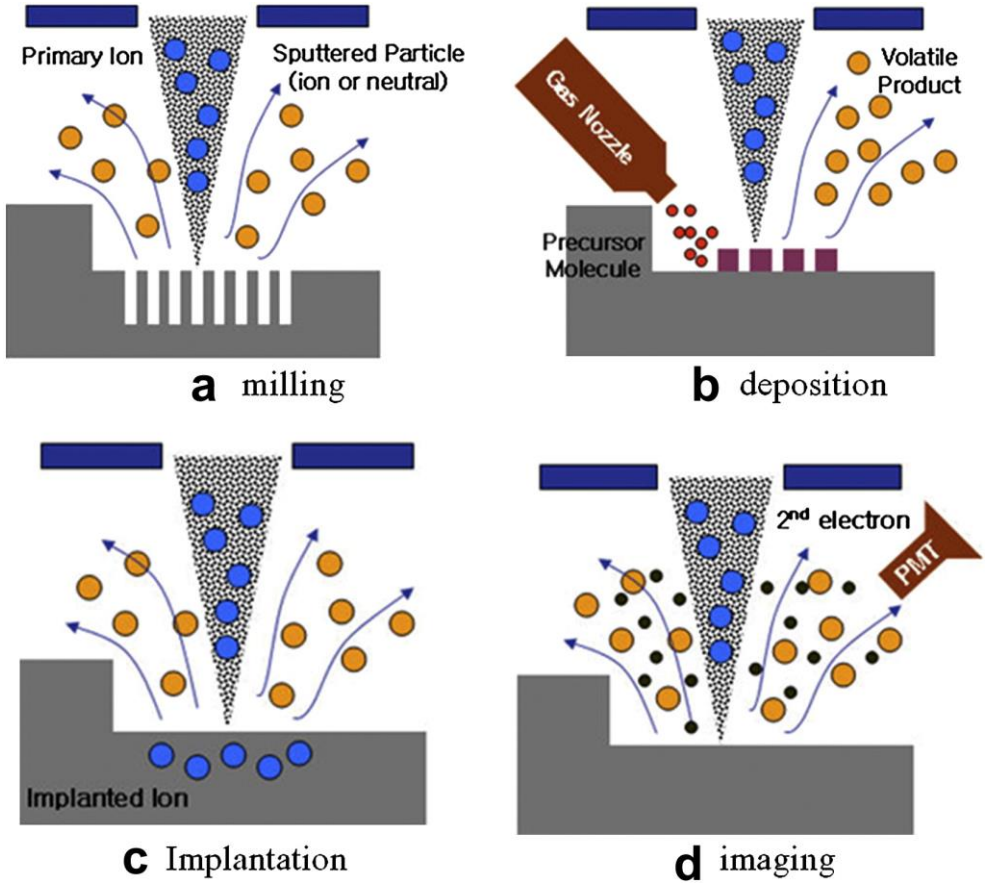

Figure 2. Schematic of FIB (a) milling, (b) deposition, (c) implantation, and (d) imaging. [46]

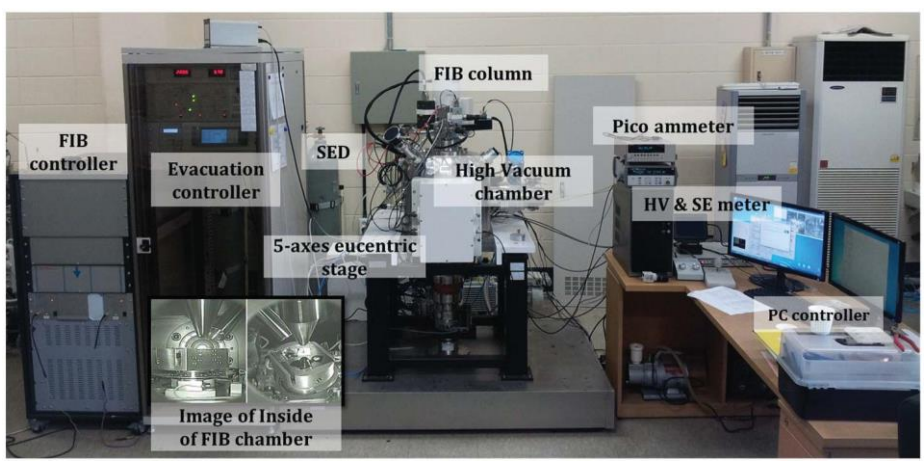

Figure 3. The system of FIB.

3.2. Design, Milling and Patterning

Using FIB milling with the aid of an in situ nanomanipulation/ characterization platform installed in the FIB system, the shape of microrobot can be fabricated. See Figure 6, the design of the microrobot is optimized exhibiting two feet and four diamond patterns, which has been already demonstrated the achievement of a good balance of adequate actuation force, weight and manufacturing simplicity from the previous study [48]. And the functionality of the microrobot can be represented by the microneedle constructed in the front of the robot in order to sting or push small objects if necessary, which can be replaced as a gripper according to the requirements.

A commercial Nitinol wire (Dynalloy, Inc. (USA)) with a diameter of 25 μm is machined into a thin plate with a thickness of 1 μm by FIB milling as illustrated in the figure. Rough milling is performed to remove most of the SMA material under high ion dose conditions to shape the structure of microrobot of one side including the foot and the side body, and then finely ground at low incident angles under lower ion beam conditions to minimize ion damage. After completing the thinning process, the sample is rotated longitudinally by 90° to perform another milling process from the top and the desired diamond-shaped frame structure is obtained by further FIB milling on this plane to gain the ability of spring-like behavior under tensile

deformation with successfully demonstrating a large elongation range compared with bulk SMA materials previously, which imparts large displacements by exploiting the scale effect, with each frame structure having a thickness of 1 μm. Due to the shape memory effect, these structures stretch under tensile stress and shrink upon heating.

After sculpting the shape of microrobot, the sample will be trained to have two-way shape memory effect. Unlike common one-way shape memory alloy, which can only remember the high temperature (austenite) shape, two-way shape memory alloy remembers both high temperature and low temperature shapes which can be trained from one-way shape memory alloy. It is believed that training process plays a key role in the introduction of two-way shape memory from an initially one-way shape memory alloy. It will be further discussed in the next session.

The sample is put back into the FIB chamber after conducting the training process. A small connecting bridge is created at the end in order to facilitate the removal of microrobot from the wire around 1 μm, which is prepared for being cut from the SMA wire to separate the robot for wireless actuation. The furnished robot exhibits 55 μm in length, 25 μm in width and 8 μm in thickness. All the milling processes with a total duration around 12 hours are concluded as Figure 7.

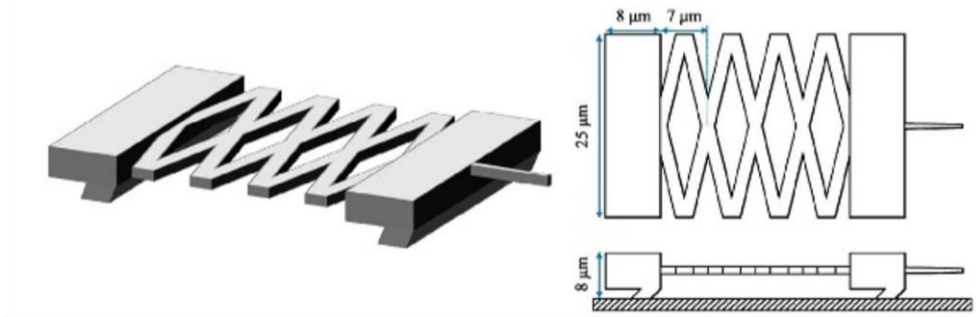

Figure 4. Schematics of microrobot.

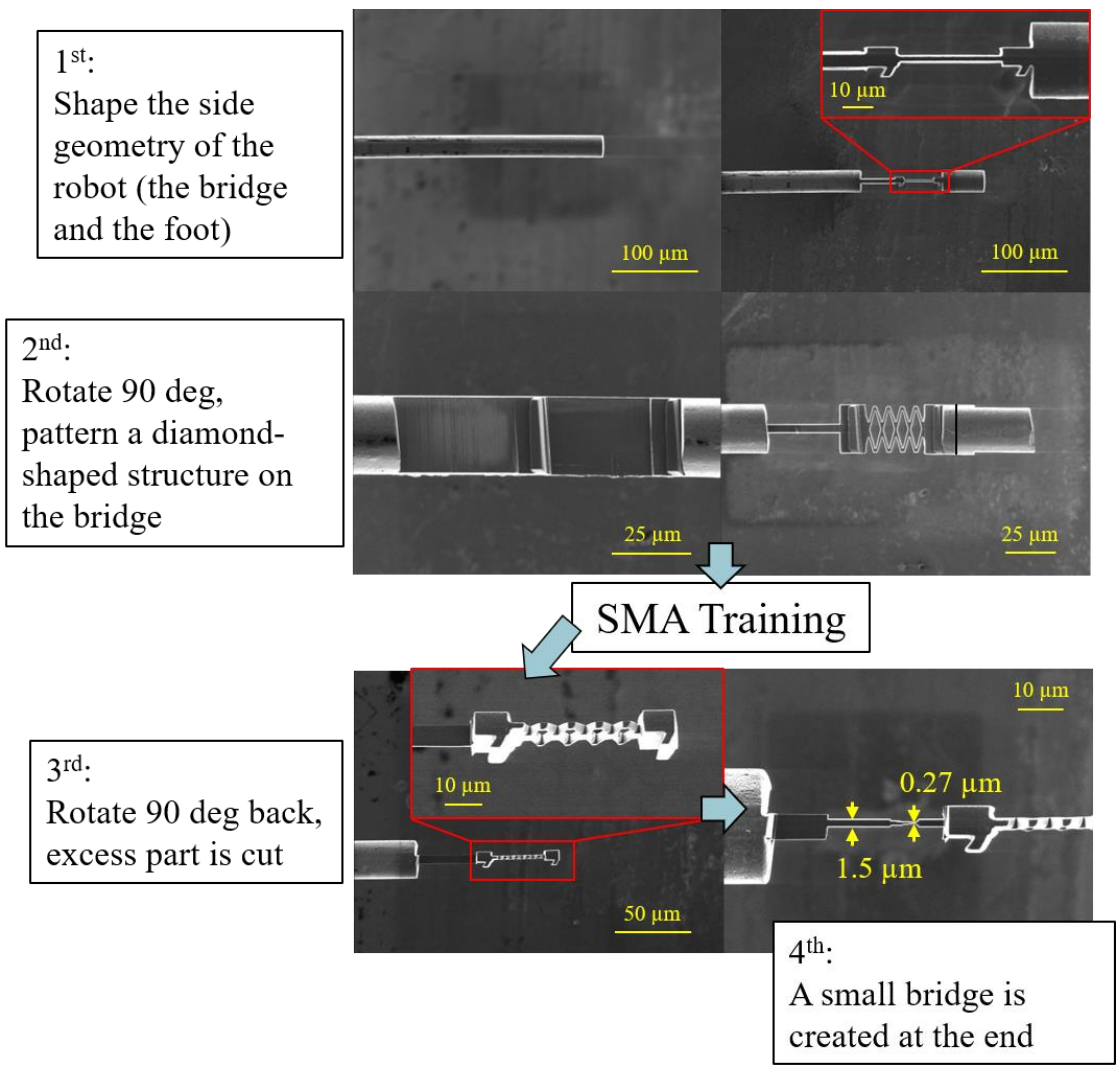

Figure 5. Prototyping process using FIB.

3.3. SMA Training

Unlike one-way shape memory alloy (OWSMA), which can only remember the high temperature (austenite) shape, two-way shape memory alloy (TWSMA) remembers both high temperature and low temperature shapes. It is believed that the training process plays a key role in the introduction of TWSMA from an initially OWSMA.

In most cases, SMAs are supplied as raw materials, i.e. without SME. To memorize a certain shape, heat treatment is normally required. This is to say, fixing the SMA into a required shape and then heating it up for a certain period of time at a high temperature. After this, OWSMA is formed. Next, the same procedure is repeated but with the different clamped shape of SMA and different heat treatment time. This is the training of TWSMA by reheat treatment.

The reheat treatment time plays an important role in obtaining the optimum two-way SME. With short reheat treatment time, specimens will adopt a shape closer to that of the shape after first heat treatment. However, the two-way SME is somehow lesser with an inappropriate treating time. Thus, the duration of reheating treatment is also necessary to be considered carefully through this approach [47].

In order to train the sample to have a two-way shape memory effect, the sample is placed under a laser scanning platform as illustrated in Figure 8. With the aid of a three-axis linear nano-manipulator (SLC-1730, SmarAct GmbH), the microgripper (SG-1730, SmarAct GmbH) is controlled to grip the shaped sample wire as the figure. With stretching the diamond-shaped frame of the microrobot with around 10 μm, the gripper is then loosened and released. Next, the patterned bridge is heat by a laser scanner to allow recovery of the original shape. This process is repeated 3 times in order to improve the shape memory effect through reheat treatment, such that the frame structure can remember a wider low temperature shape providing a larger tensile deformation. The whole training processes are concluded in Figure 9.

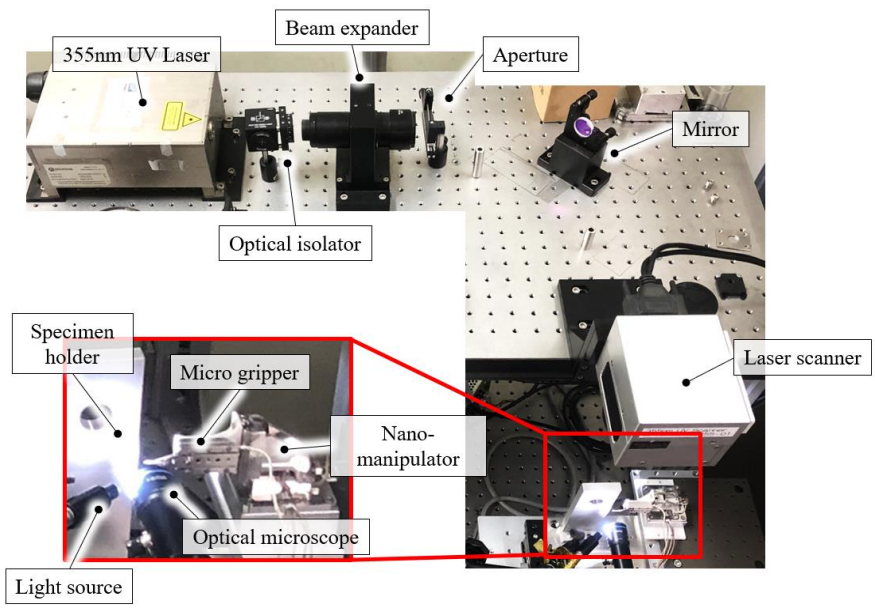

Figure 6. Experimental setup of the laser system for training the microrobots

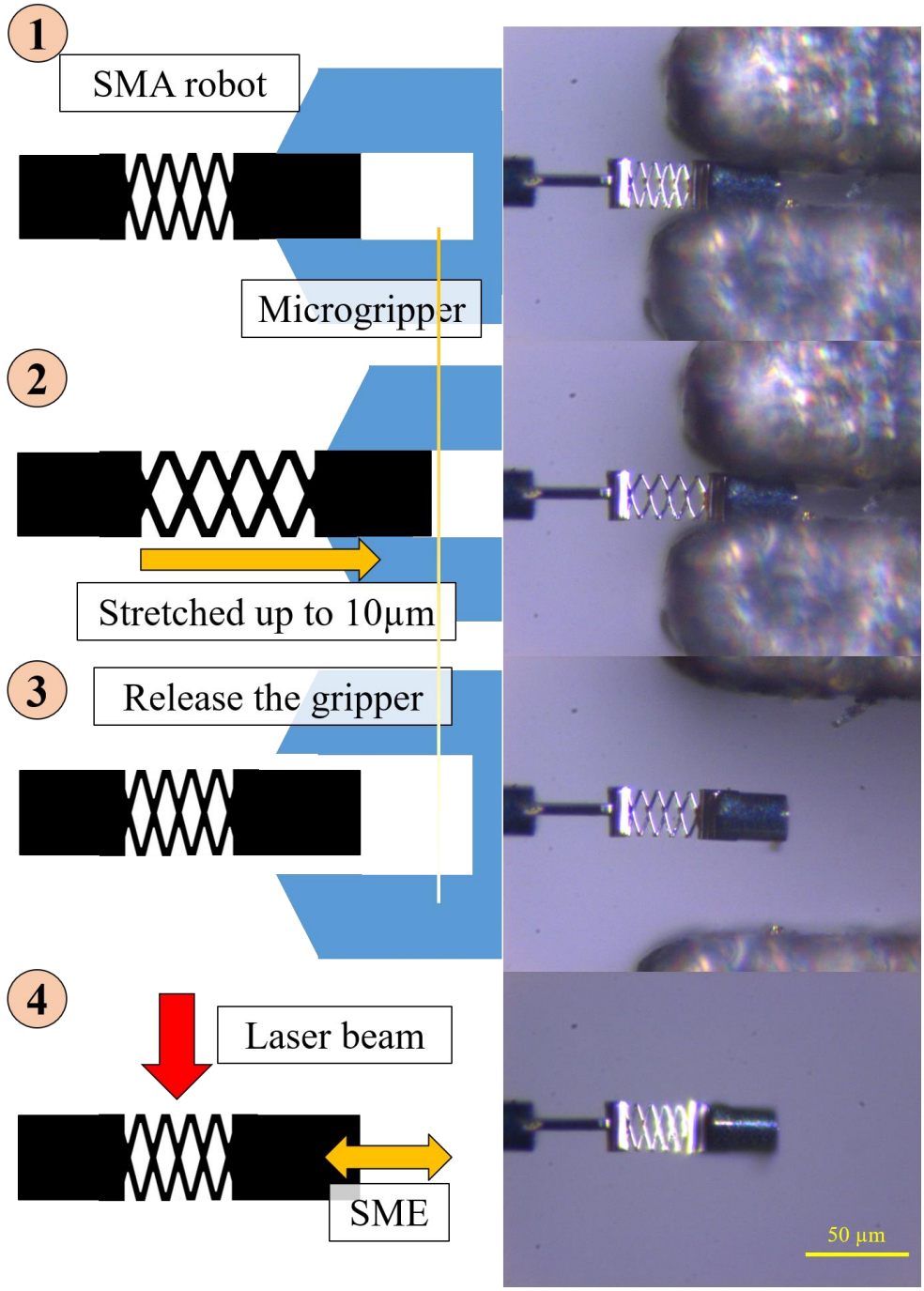

Figure 7. Training process of the two-way SME.

3.4. Localization

Since the size of the SMA microrobot is too small which cannot be observed with human eyes directly, a stable separation treatment is necessary to prevent from the risk of losing the microrobot. If just simply cut the robot and make it drop freely to the platform, instead of an unpredictable chance to receive it safely without being affected by the environmental factors such as airflow caused by ventilation, it is also impossible to arrange the microrobot to the desired position.

For this case, a temporary adhesive is used for securing the microrobot. When the extremely thin connecting bridge is created, the microrobot sample can be taken out from the chamber and attached to the separation setup. A cover glass, which is the targeted platform of placing the robot, is laid on a heater with temperature control module with a small amount of solid Aquabond ™ Temporary Adhesive (Aquabond Technologies) with a melting point of 55°C, which can be dissolved in hot water or hot ethyl alcohol. Raising the temperature of the platform up to 70°C for the purpose of making a fully melted adhesive is followed by dipping the microrobot into the liquid adhesive. With the aid of the adhesive, the microrobot can be attached to the desired location positioned by the nano manipulator. Cooling is the next step to solidify the adhesive and make a secure adherence to the glass platform. As the robot is stuck strong and tight, when the pulling force

generated from the movement of the nano manipulator is great enough to break the extremely thin connecting bridge, fracture occur and the microrobot can be separated from the sample holder. A firm localization of placing microrobots at the right positions is achieved (see Figure 12).

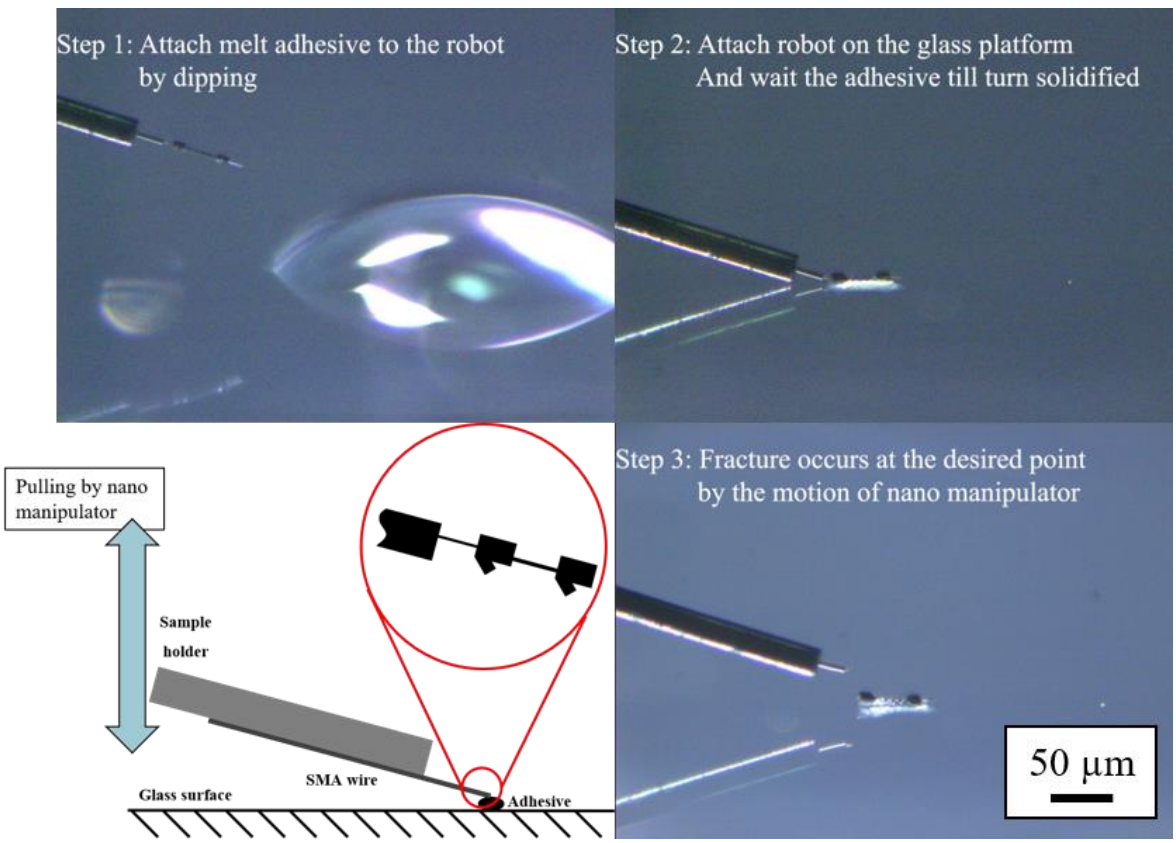

Figure 8. Schematic of the procedures for the separation of microrobot.

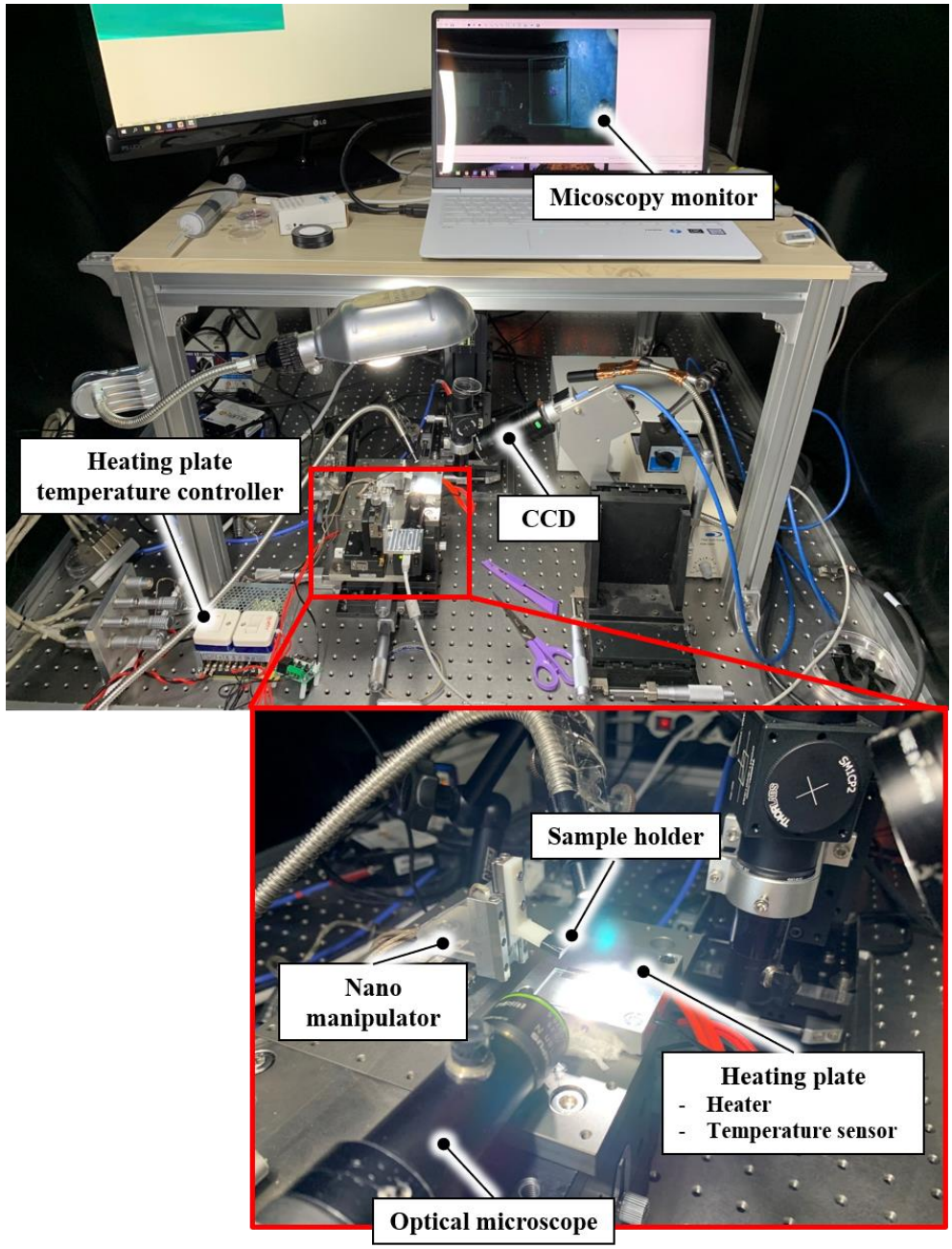

Figure 9. Experimental setup of separation of microrobot.

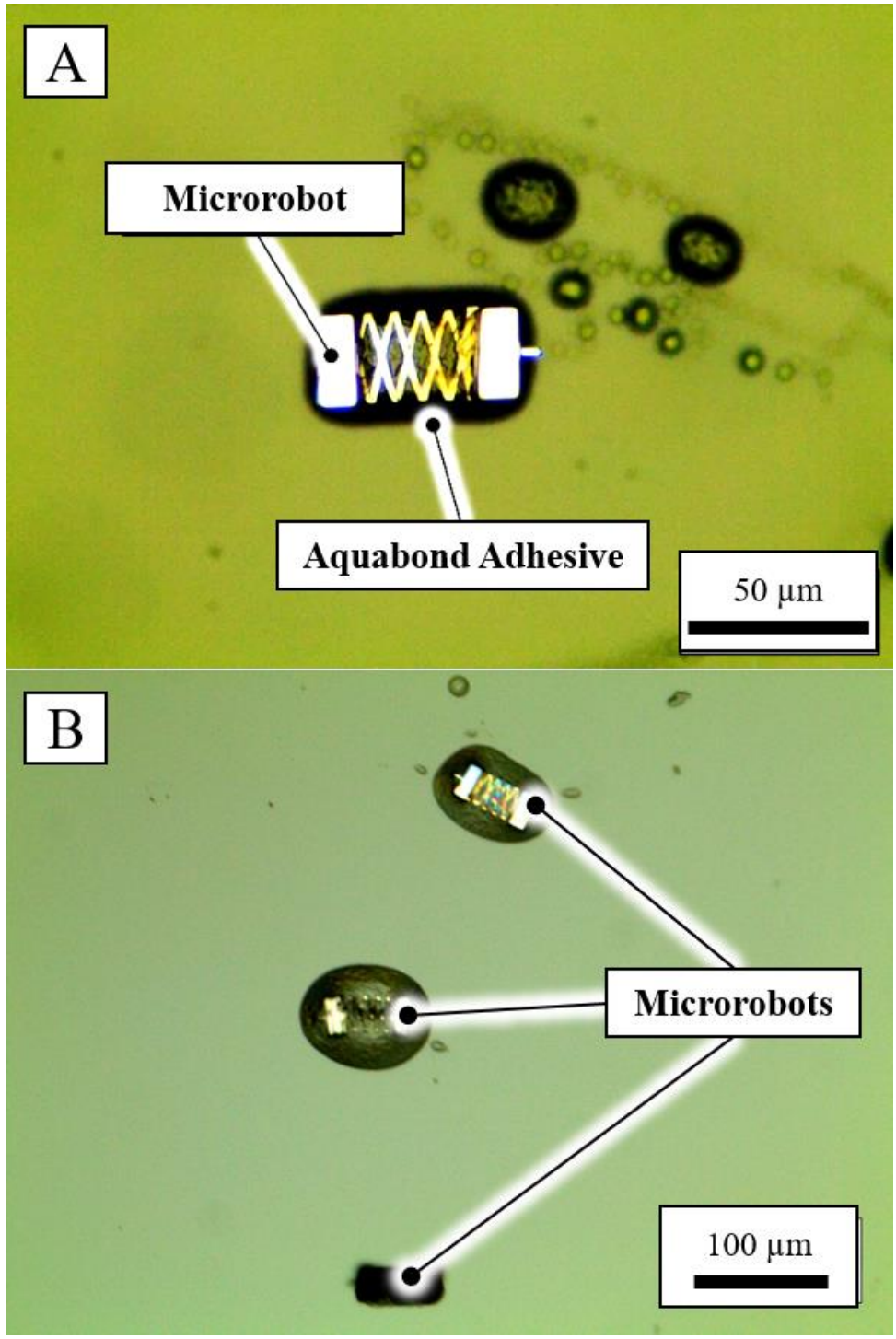

Figure 10. The microrobots localizing with temporary Aquabond adhesive.

Chapter 4. Laser scanning operation

4.1. Laser Activation Mechanism and Experimental Setup

The attached temporary Aquabond adhesive can be removed by hot water or warm ethyl alcohol (~60°C), making the SMA microrobot being available to be actuated. Due to the density of the SMA which is higher than most liquids, the robot can sink to the ground and crawl under laser activation when it is immersed in ethyl alcohol on the control platform (see Figure 13). In order to activate the microrobot, the controllable nanosecond, pulsed laser beam passing through the Galvano laser scanner is projected on the upper surface of the robot, allowing the energy to transfer as the thermal energy for the actuation of SMA, under the observation from the CCD camera in the bottom of the 3D printed jig. The laser power is monitored frequently by the power meter to stabilize between 30 to 40 mW, avoiding inappropriate actuation or damage to the structure of the robot brought by the underpowered or overpowered laser beam.

Inspired by the crawling motion of shrimp, when the laser beam is scanned from the back to the front of the robot, the optical energy is converted to thermal energy during the irradiation, the robot can move forward with the force induced by the two-way SME and the thermophoretic effect as shown in Figure 14a and b, propelling itself with the aid of the back foot as a

leverage point, which is similar to the shrimp crawling with pushing against the bottom with the legs as propulsion. This method has advantages in untethered energy transfer for moving robots, providing a simpler control algorithm and tools than magnetic levitation. As illustrated in Figure 14c, a microrobot was activated along a direct straight continuous laser scan at a laser scanning speed of 80 mm s^{-1} and a laser scan size of 1 mm with a power of 35 mW, moving forward with an average velocity of 37.5 μm s^{-1}.

From the result, we can see that the robot followed the laser scanning from the left to the right, which can be concluded that the direction of laser scanning can control the direction of the actuation of the robot. With tilting the laser beam path, the robot can rotate according to the alignment and keep on the movement adhering to the track of the laser beam. Based on this phenomenon, with furnishing and optimizing the algorithm of constructing the laser beam path, it is assumed the maneuverability of controlling the microrobot can be improved, without considering any flaw appeared on the mechanical structure of the microrobot during fabrication such as imbalance occurred on the feet or the mass of the robot. But the energy transfer can be blocked or weakened by the obstacles and the performance of the robot can be degraded by sustained long heating leading to the inability to maintain SME.

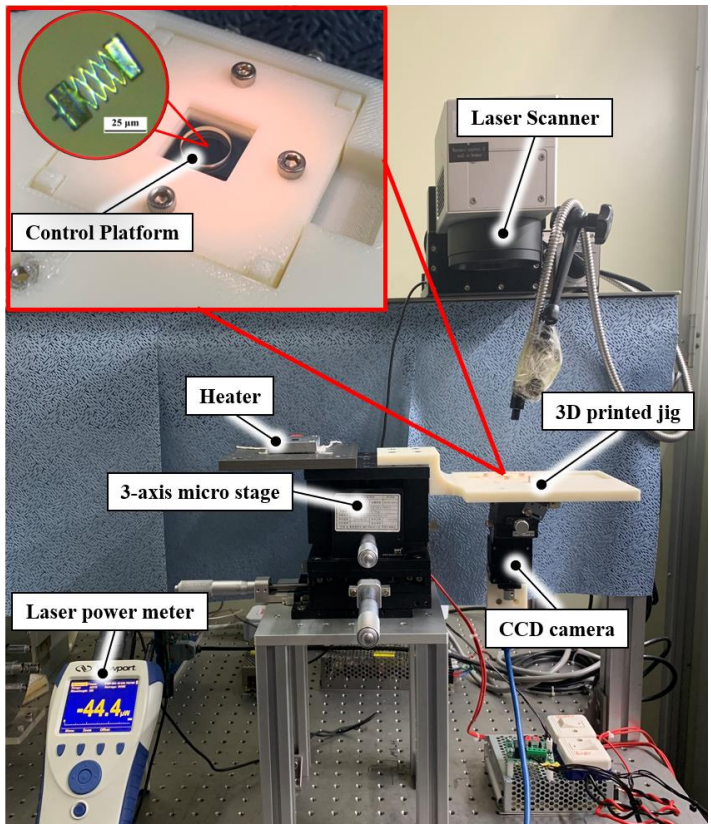

Figure 11. Experimental setup of controlling SMA microrobot.

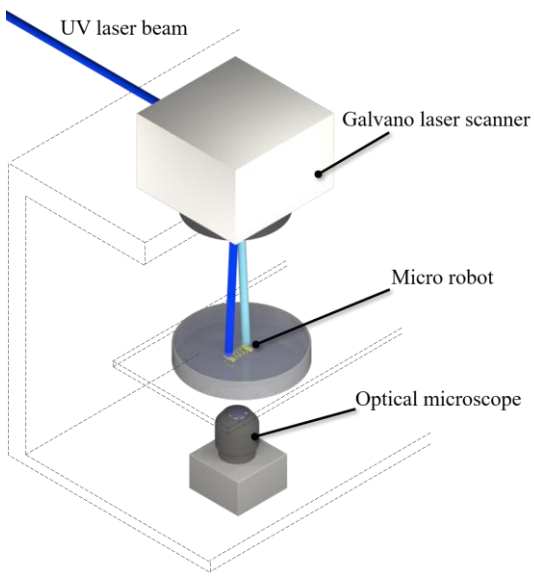

Figure 12. Schematics of the setup of laser control.

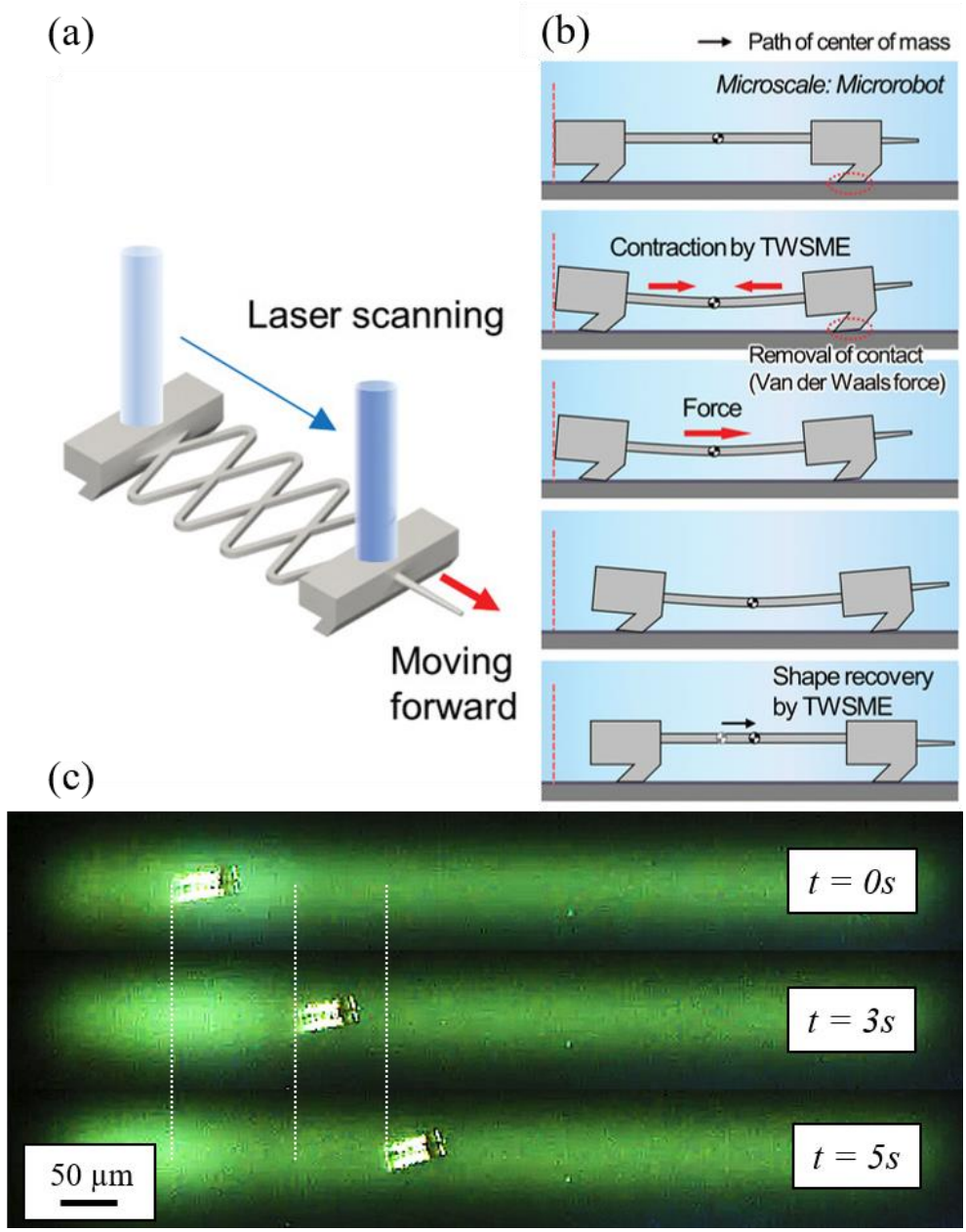

Figure 13. (a) The schematic of the methodology to activate the microrobot. (b) Actuation mechanism mimicking the crawling motion of shrimps. (c) Forward linear motion within 5 s at a velocity of 37.5 μm s^{-1}.

4.2. Parameter Study for optimization

From the previous study, there is an optimal performance in the actuation speed of the microrobot with corresponding laser controlling parameter (e.g. the laser scanning speed, the scan size of the laser beam and the laser power). Different combinations of the laser scanning speed (from 10 – 80 mm s^{-1}) and the laser power (from 40 – 60 mW) were chosen to evaluate the maximum actuation speed of the SMA microrobot. It was discovered that the microrobot can move faster at a higher power with a lower scanning speed and a lower power with a higher scanning speed. Although the speed of the microrobot can reach at the speed in the scale of centimeter per second at a high laser power with a low scanning speed, bubbles were generated in the media (ethyl alcohol) of the control platform when the laser beam hit the microrobot due to the high temperature, which lead to ungovernable motion of the microrobot as an adverse drawback.

Since the scan size of the laser beam was fixed as 10 mm in the last study which can be an important factor fluctuating the velocity of the SMA microrobot. At this time, the laser power is fixed at 35 mW, the performance of the actuation speed with different combinations of the laser scanning speed (from 10 – 320 mm s^{-1}) and the scan size (from 1 – 10 mm) is measured and analyzed.

From the plot (See Figure 15) and Table 3, with minimizing the scan size of the laser beam, the actuation speed of the microrobot can be extremely improved, which can reach a maximum speed at 150.06 μm s^{-1} that is 15 times faster than the previous study where the scan size is 10 mm. At different scan sizes, the actuation velocity of the robot has got the peak values at a laser scanning speed of 40 mm s^{-1}. Figure 16 compares the displacement change of the motion of the robot in different scan sizes of the laser beam within 1 s, where the scanning speed is 40 mm s^{-1}. Thus, in order to maximize the performance of the robot in actuation speed, the scan size should be restricted and well-designed according to the designated laser path. With increasing the laser scanning frequency, the propulsion speed of the SMA microrobot can be greatly enhanced in different laser scanning speeds.

For some cases that the robot is being activated under extreme high laser scanning speed like 320 and 640 mm s^{-1}, there is no any movement on the robot which can be due to the insufficient energy transferred from the laser or lacking enough time for martensitic transformation of SMA in changing between two different memorized shapes.

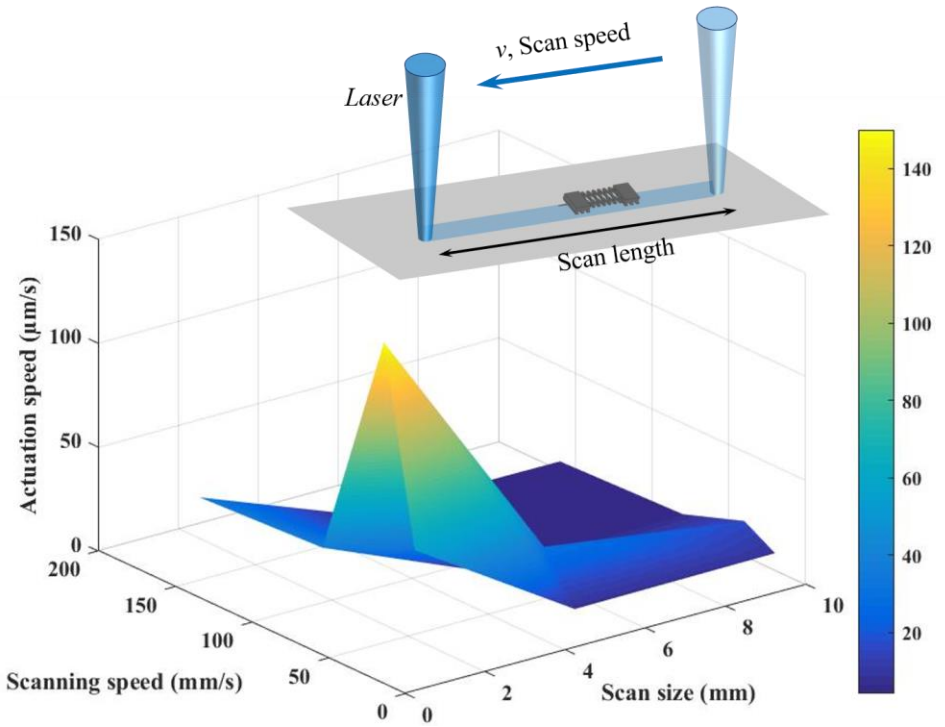

Figure 14. Actuation velocity of the microrobot in different combinations of laser scanning speeds and scan sizes (in μm s^{-1}).

		Laser scanning speed (mm s^{-1})					
		10	20	40	80	160	320
Scan size (mm)	1	47.86	56.93	150.06	37.5	34.25	No movement
	5	Bubble generation	7.48	30.56	5.04	4.67	No movement
	10	Bubble generation	8.01	14.65	6.19	4.10	3.70

Table 3. Summarization of the measured data of the actuation velocity of the microrobot (in μm s^{-1}).

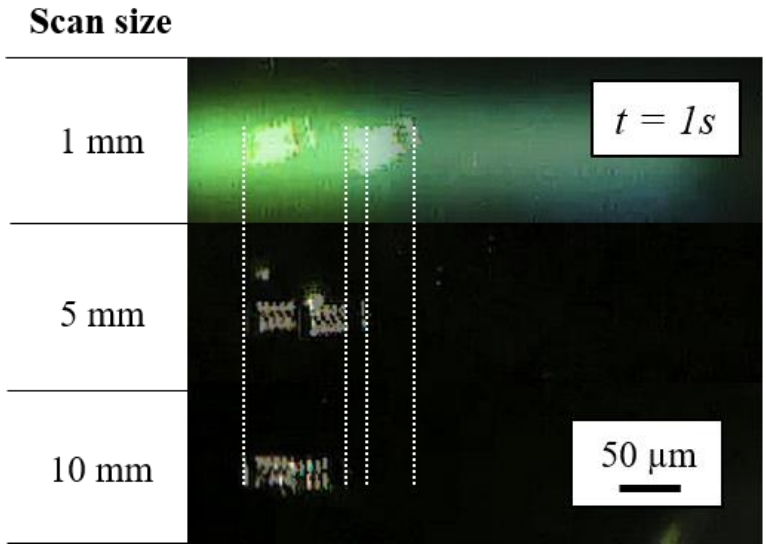

Figure 15. Comparison of the displacement change of the motion of the robot in different scan sizes of the laser beam within 1 s, where the scanning speed is 40 mm s^{-1} and the laser power is 35 mW.

4.3. Demonstration of different designated path

The maneuverability of the SMA microrobot can be exhibited in this session. Despite the linear motion shown in the last session, different laser paths have been designed to demonstrate the ability of the microrobot to follow the laser path. Alphabet ‘U’, ‘S’ and number ‘2’ are chosen as the laser pathway (see Figure 17). The reason why choosing these characters as designated laser pathways is to show the ability of the robot to follow a curve and to rotate instantly at a turnpoint.

The character pathways are made by a continuous scanning following one direction indicated by the blue arrows shown in the figure, with the laser power of 35 mW and the laser scanning speed at 100 mm s^{-1} in which a stable robot actuation can be performed according to the result of the parameter study. Since all the scanning is made without dividing the pathway into different pieces to maximize the actuation velocity of the robot, the duration to complete following the different designated paths ranges from 31 s to 80 s as the scan size of different characters are different. It is successfully demonstrated that the robot can complete the designated tracks.

In addition, the solution to the Königsberg bridge problem (see Figure 18a) is also considered as an intricate pathway which consists of different complex scanning roads. The pathway is constructed according to Figure

18b by following the number order as the direction of the laser beam. Since the scan size would be extremely long which can lead to insufficient energy transferred causing non-movement of the robot, the pathway is divided into different sessions. The motion with time to solve the bridge problem is shown in Figure 18c.

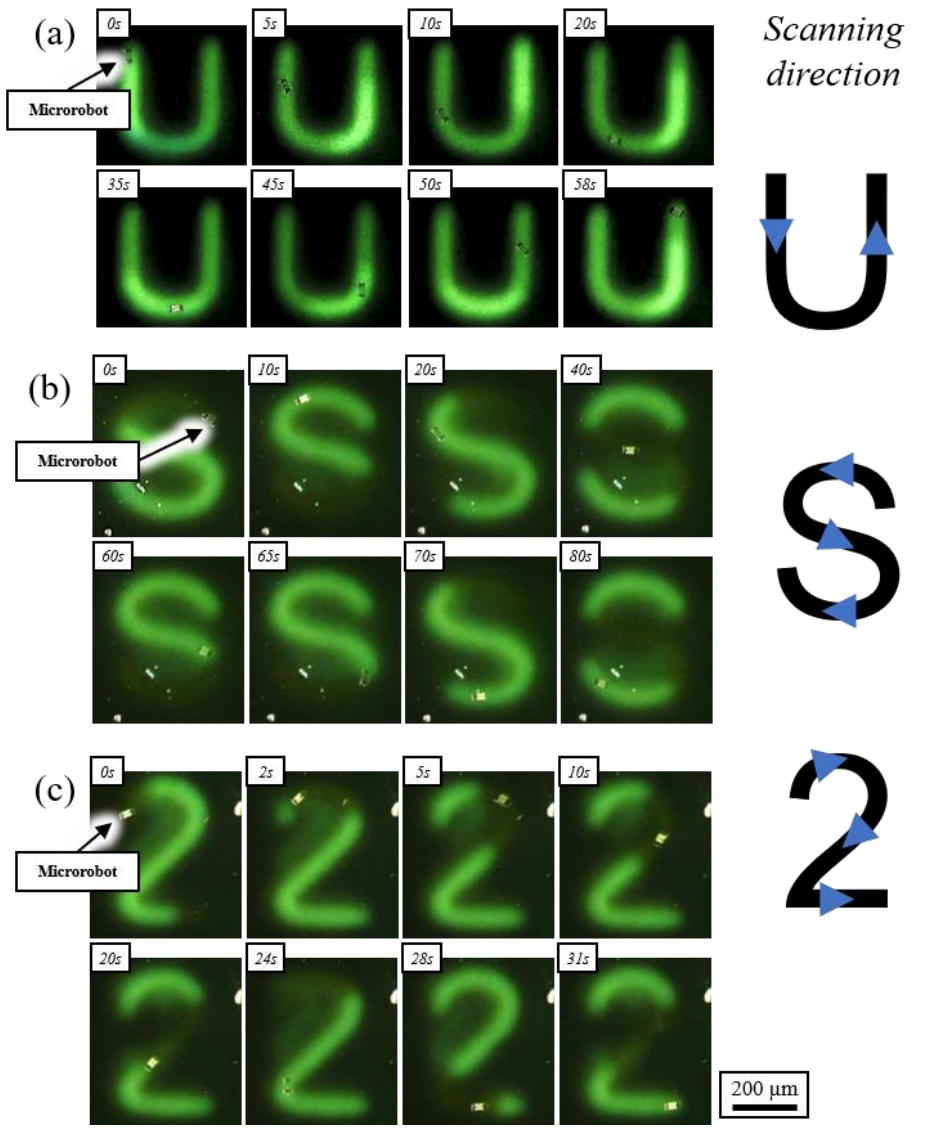

Figure 16. Different designated pathways, (a) alphabet ‘U’, (b) alphabet ‘S’, (c) number ‘2’.

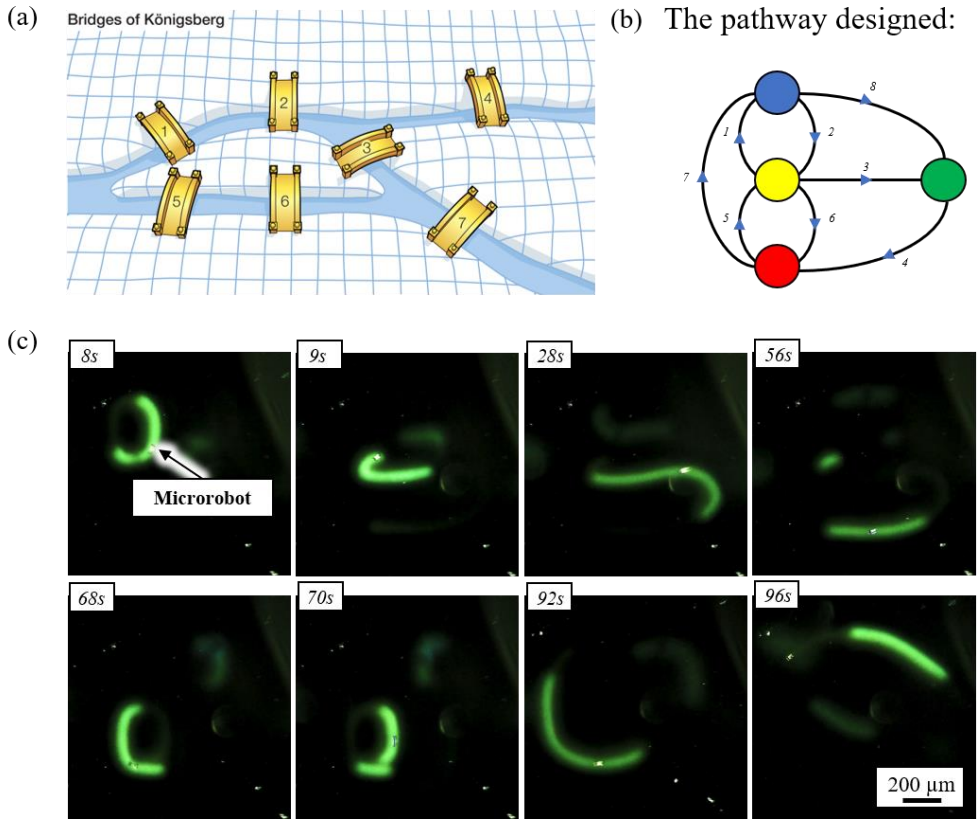

Figure 17. (a) The Königsberg bridge problem. (b) The designed solution laser pathway with the order of number as the direction. (c) The motion of the microrobot with time indicated.

4.4. Swarm operation of multiple microrobots

Swarm control is a hot topic in the world of microrobots. It is hard to find the functionality of controlling one microrobot to perform tasks in any environments. Especially in microenvironment, different microorganisms or particles with different shapes and sizes exist and form different obstacles, it is insufficient to carry out missions with using one robot to face various situations occurred in an extreme small working place. Collaborations of numerous microrobots is the main issue to be realized now.

In order to demonstrate the operation of multiple microrobots, several microrobots are placed on the same workspace (see Figure 12). We firstly achieve a linear motion of two robots as illustrate in Figure 19, in which two robots are activated simultaneously at the same time and reached the end of the designated laser pathway, which can be used to arrange and align the positions of the microrobots. There is one notable thing that each robot has its optimal controlling parameters. With using the same parameter to operate the laser, two microrobots actuate at different velocity which can be due to the shortage of the FIB manufacturing process as the flatness of the milling surface is greatly affected by the limited resolution of the FIB. As mentioned, there is a chance that defects can be observed on the mechanical structure of the microrobot such as imbalance occurred on the feet or the

mass of the robot, which can lead to improper propulsion without following the correct laser path such as self-rotation.

Despite linear forward movement, we have increased the complexity of the laser pathway. A combination of the special character '♡', and the alphabet 'U' are designed as the laser pathways. From Figure 20b, the overall movement of microrobot with timeline is showed and the overall duration to complete the specific tracks is around 1 min. With appropriate laser control parameter with a high laser scanning speed around 80 – 100 mm s^{-1}, the accidents of being out of track due to bubbles generation can be avoided.

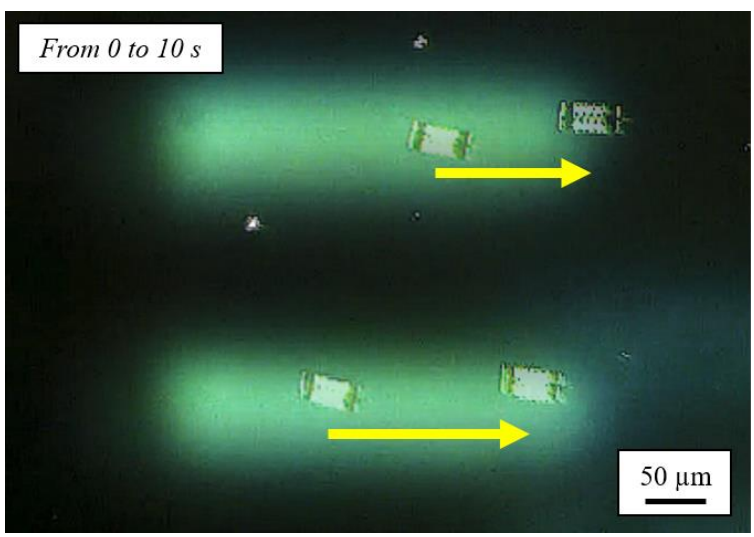

Figure 18. The linear forward movement of two microrobot activated at the same time.

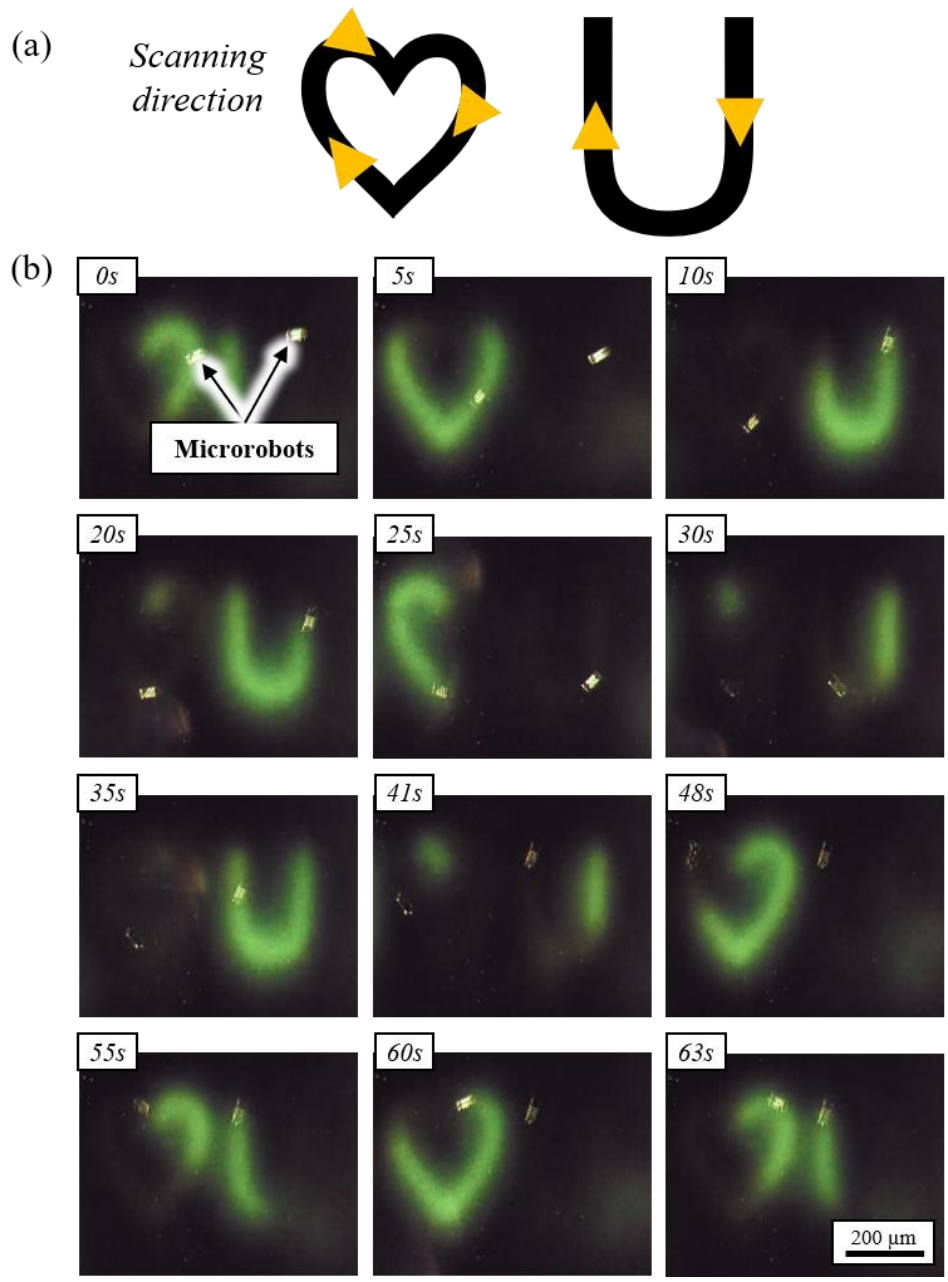

Figure 19. (a) The designed pathway consisting of a special character '♡', and an alphabet 'U' with indicated blue arrows as the laser scanning direction. (b) The actual movement of two microrobots with time indicated.

4.5. Discussion about Swarm Control

There is a scanning sequence during activating multiple robots. To control two microrobots travelling for 1 mm respectively, a total scan size is 2 mm leading to longer time for complete to travel the pathway. In order to optimize the performance of both robots, the designed pathway should be divided into different pieces, which is similar to Figure 18. Such that, in assumption, if the total scan size of the respective pathways to control different robot is restricted to 1 mm each time, they can all exhibit a maximum speed as 150 μm s^{-1} when the scanning speed is 40 mm s^{-1}.

To estimate the maximum number of the robots that can be controlled at the same time, a simple evaluation has been done. Assume that an effective motion of a robot with a relevant effect speed, 10 μm s^{-1}, which is the same as the optimal speed in the previous study. And take the optimal laser scanning parameter from Table 3, when the total scanning size of all the robots is restricted as 1 mm, it is assumed that all the robots can exhibit 150 μm s^{-1}. The time needed for travelling 10 μm defined as an effective travelling distance for each microrobot is calculated as Figure 20. Without considering the limited rotation rate of the mirror in Galvano laser scanner, the time needed is proportional to the number of the robots. A valid swarm motion can be defined when the robots can complete the designed distance in 1 s, that the maximum number of the robots which can be controlled is

fifteen. Such that, it is estimated that the independent motions of 15 robots can be performed within 1 s, which can bring out a similar effect as giving different commands to different independent robots, that can be concluded as swarm. With the improvement in the control algorithm, the scanning pathway can be designed to shorten the scanning length to maximize the speed of the robot under a stable laser scanning frequency.

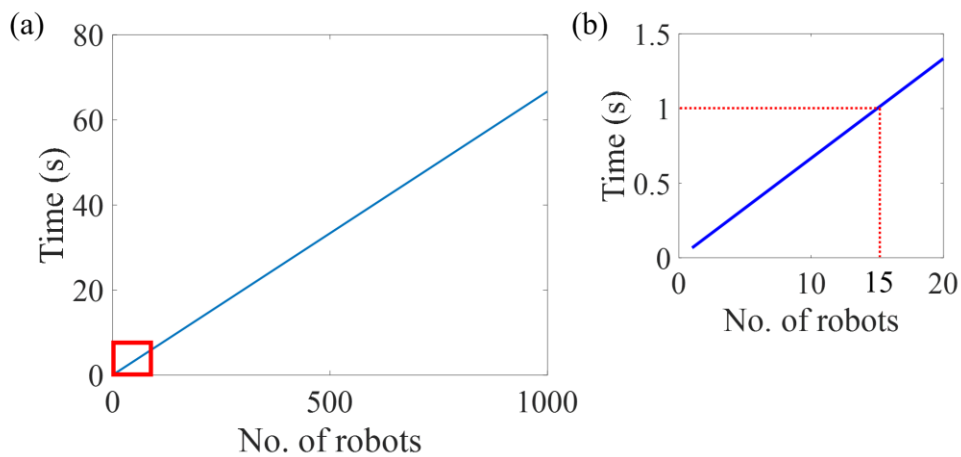

Figure 20. The time needed for travelling 10 μm for each microrobots, a) the size of the number of robots: 1 to 1000, b) the size of the number of robots: 1 to 20.

Chapter 5. Conclusion

In this study, we designed and fabricated a SMA microrobot through FIB milling. With training the microrobot to have a two-way SME, the robots can gain the ability to be actuated under laser scanning with high frequency. The actuation velocity can be maximized with shortening the scan size of the laser beam, with the improved manufacturing process, the performance in speed can achieve 15 times faster than before.

A basic and simple swarm control methodology has been constructed successfully to manipulate multiple SMA microrobots to perform different accurate and precise designated actuation motions such as linear motion, bending motion, rotation, and torsion. The direction of laser scanning can control the direction of the actuation of the robot, a high maneuverability of controlling the microrobots can be realized with assigning specific laser beam pathways to lead the robots to reach the targeted destinations.

The ability to pick up, transport, and release diverse cargoes plays an important role in numerous practical applications in the environmental and biomedical areas, which should be further explored in the future. Biopsy or delivering particles can be expected and performed with the collaboration of multiple robots under a sophisticated laser scanning method with determining appropriate routes, allowing more variability and

diversifications on the solutions to implement microrobots with high steerability in order to overcome the existing challenges in microenvironment. A more accurate and precise fabrication methodology without affecting the structure of the robot should be considered as well.

Bibliography

1. Sitti, M., Ceylan, H., Hu, W., Giltinan, J., Turan, M., Yim, S., & Diller, E, *Biomedical applications of untethered mobile milli/microrobots*, Proceedings of the IEEE, 103(2), 205-224. (2015).
2. Ceylan, H., Giltinan, J., Kozielski, K., & Sitti, M., *Mobile microrobots for bioengineering applications*, Lab on a Chip, 17(10), 1705-1724. (2017).
3. Sitti, M., *Miniature devices: Voyage of the microrobots*, Nature, 458(7242), 1121. (2009).
4. Nelson, B. J., Kaliakatsos, I. K., & Abbott, J. J., *Microrobots for minimally invasive medicine*, Annual review of biomedical engineering, 12, 55-85. (2010).
5. Edd, J., Payen, S., Rubinsky, B., Stoller, M. L., & Sitti, M., *Biomimetic propulsion for a swimming surgical micro-robot*, In Proceedings 2003 IEEE/RSJ International Conference on Intelligent Robots and Systems (IROS 2003) (Cat. No. 03CH37453), Vol. 3, pp. 2583-2588. (2003).
6. Kim, Y., Parada, G. A., Liu, S., & Zhao, X, *Ferromagnetic soft continuum robots*, Science Robotics, 4(33), eaax7329. (2019).
7. Chen, X. Z., Jang, B., Ahmed, D., Hu, C., De Marco, C., Hoop, M., Mushtaq, F., Nelson, B. J., & Pané, S., *Small-Scale Machines Driven by External Power Sources*, Advanced Materials, 30(15), 1705061. (2018).
8. Parmar, J., Ma, X., Katuri, J., Simmchen, J., Stanton, M. M., Trichet-Paredes, C., Soler, L., & Sanchez, S., *Nano and micro architectures for self-propelled motors*, Science and technology of advanced materials, 16(1), 014802. (2015).
9. Sánchez, S., Soler, L., & Katuri, J., *Chemically powered micro-and nanomotors*, Angewandte Chemie International Edition, 54(5), 1414-1444. (2015).

10. Wang, W., Duan, W., Ahmed, S., Sen, A., & Mallouk, T. E, *From one to many: Dynamic assembly and collective behavior of self-propelled colloidal motors*, Accounts of chemical research, 48(7), 1938-1946. (2015).
11. Wang, H., & Pumera, M., *Fabrication of micro/nanoscale motors*, Chemical reviews, 115(16), 8704-8735. (2015).
12. Xu, T., Gao, W., Xu, L. P., Zhang, X., & Wang, S., *Fuel-free synthetic micro-/nanomachines*, Advanced Materials, 29(9), 1603250. (2017).
13. Chen, X. Z., Hoop, M., Mushtaq, F., Siringil, E., Hu, C., Nelson, B. J., & Pane, S., *Recent developments in magnetically driven micro-and nanorobots*, Applied Materials Today, 9, 37-48. (2017).
14. Medina-Sánchez, M., Schwarz, L., Meyer, A. K., Hebenstreit, F., & Schmidt, O. G., *Cellular cargo delivery: Toward assisted fertilization by sperm-carrying micromotors*, Nano letters, 16(1), 555-561. (2015).
15. Hosseinidoust, Z., Mostaghaci, B., Yasa, O., Park, B. W., Singh, A. V., & Sitti, M., *Bioengineered and biohybrid bacteria-based systems for drug delivery*, Advanced drug delivery reviews, 106, 27-44. (2016).
16. Huber, J. E., Fleck, N. A., & Ashby, M. F., *The selection of mechanical actuators based on performance indices*, Proceedings of the Royal Society of London. Series A: Mathematical, physical and engineering sciences, 453(1965), 2185-2205. (1997).
17. Krulevitch, P., Lee, A. P., Ramsey, P. B., Trevino, J. C., Hamilton, J., & Northrup, M. A., *Thin film shape memory alloy microactuators*, Journal of microelectromechanical systems, 5(4), 270-282. (1996).
18. Bell, D. J., Lu, T. J., Fleck, N. A., & Spearing, S. M., *MEMS actuators and sensors: observations on their performance and selection for purpose*, Journal of Micromechanics and Microengineering, 15(7), S153. (2005).

19. Shin, D. G., Kim, T. H., & Kim, D. E., *Review of 4D printing materials and their properties*, International Journal of Precision Engineering and Manufacturing-Green Technology, 4(3), 349-357. (2017).
20. Choudhary, N., & Kaur, D., *Shape memory alloy thin films and heterostructures for MEMS applications: a review*, Sensors and Actuators A: Physical, 242, 162-181. (2016).
21. Fu, Y., Du, H., Huang, W., Zhang, S., & Hu, M., *TiNi-based thin films in MEMS applications: a review*, Sensors and Actuators A: Physical, 112(2-3), 395-408. (2004).
22. Kahn, H., Huff, M. A., & Heuer, A. H., *The TiNi shape-memory alloy and its applications for MEMS*, Journal of Micromechanics and Microengineering, 8(3), 213. (1998).
23. Wang, W., & Ahn, S. H., *Shape memory alloy-based soft gripper with variable stiffness for compliant and effective grasping*, Soft robotics, 4(4), 379-389. (2017).
24. Wang, W., Rodrigue, H., Kim, H. I., Han, M. W., & Ahn, S. H., *Soft composite hinge actuator and application to compliant robotic gripper*, Composites Part B: Engineering, 98, 397-405. (2016).
25. Rodrigue, H., Wang, W., Han, M. W., Kim, T. J., & Ahn, S. H., *An overview of shape memory alloy-coupled actuators and robots*, Soft robotics, 4(1), 3-15. (2017).
26. Kim, B., Lee, M. G., Lee, Y. P., Kim, Y., & Lee, G., *An earthworm-like micro robot using shape memory alloy actuator*, Sensors and Actuators A: Physical, 125(2), 429-437. (2006).
27. Villanueva, A. A., Joshi, K. B., Blottman, J. B., & Priya, S., *A bio-inspired shape memory alloy composite (BISMAC) actuator*, Smart Materials and Structures, 19(2), 025013. (2010).
28. Yuan, H., Fauroux, J. C., Chapelle, F., & Balandraud, X., *A review of rotary actuators based on shape memory alloys*, Journal of Intelligent Material Systems and Structures, 28(14), 1863-1885. (2017).

29. Jani, J. M., Leary, M., Subic, A., & Gibson, M. A., *A review of shape memory alloy research, applications and opportunities*, Materials & Design (1980-2015), 56, 1078-1113. (2014).
30. Morgan, N. B., *Medical shape memory alloy applications—the market and its products*, Materials Science and Engineering: A, 378(1-2), 16-23. (2004).
31. Hodgson, D. E., Wu, M. H., & Biermann, R. J., *Shape Memory Alloys*, Properties and Selection: Nonferrous Alloys and Special-Purpose Materials, ASM International, Vol. 2, 897-902. (1990).
32. Sun, L., & Huang, W. M., *Nature of the multistage transformation in shape memory alloys upon heating*, Metal Science and Heat Treatment, 51(11), 573-578. (2009).
33. Hou, M. T., Shen, H. M., Jiang, G. L., Lu, C. N., Hsu, I. J., & Yeh, J. A., *A rolling locomotion method for untethered magnetic microrobots*, Applied Physics Letters, 96(2), 024102. (2010).
34. Floyd, S., Pawashe, C., & Sitti, M., *Two-dimensional contact and noncontact micromanipulation in liquid using an untethered mobile magnetic microrobot*, IEEE Transactions on Robotics, 25(6), 1332-1342. (2009).
35. Yesin, K. B., Vollmers, K., & Nelson, B. J., *Modeling and control of untethered biomicrorobots in a fluidic environment using electromagnetic fields*, The International Journal of Robotics Research, 25(5-6), 527-536. (2006).
36. Donald, B. R., Levey, C. G., McGray, C. D., Paprotny, I., & Rus, D., *An untethered, electrostatic, globally controllable MEMS micro-robot*, Journal of microelectromechanical systems, 15(1), 1-15. (2006).
37. Khamesee, M. B., Kato, N., Nomura, Y., & Nakamura, T., *Design and control of a microrobotic system using magnetic levitation*, IEEE/ASME transactions on mechatronics, 7(1), 1-14. (2002).

38. Gill, J. J., Chang, D. T., Momoda, L. A., & Carman, G. P., *Manufacturing issues of thin film NiTi microwrapper*, Sensors and Actuators A: Physical, 93(2), 148-156. (2001).
39. Ali, M. S. M., Bycraft, B., Bsoul, A., & Takahata, K., *Radio-controlled microactuator based on shape-memory-alloy spiral-coil inductor*, Journal of Microelectromechanical Systems, 22(2), 331-338. (2012).
40. Takeuchi, S., & Shimoyama, I., *A three-dimensional shape memory alloy microelectrode with clipping structure for insect neural recording*, Journal of Microelectromechanical Systems, 9(1), 24-31. (2000).
41. King, A. M., Loiselle, D. S., & Kohl, P., *Force generation for locomotion of vertebrates: Skeletal muscle overview*, IEEE Journal of Oceanic Engineering, 29(3), 684-691. (2004).
42. Miriyev, A., Stack, K., & Lipson, H., *Soft material for soft actuators*, Nature communications, 8(1), 596. (2017).
43. Lee, H. T., Kim, M. S., Lee, G. Y., Kim, C. S., & Ahn, S. H., *Microscale Actuation: Shape Memory Alloy (SMA)-Based Microscale Actuators with 60% Deformation Rate and 1.6 kHz Actuation Speed*, Small, 14(23), 1870104. (2018).
44. Pawashe, C., Floyd, S., & Sitti, M., *Multiple magnetic microrobot control using electrostatic anchoring*, Applied Physics Letters 94, 164108. (2009).
45. Folch, A., *Introduction to BioMEMS*, CRC Press. (2013).
46. Kim, C. S., Ahn, S. H., & Jang, D. Y., , Vacuum, 86(8), 1014-1035. (2012).
47. Huang, W., & Toh, W., *Training two-way shape memory alloy by reheat treatment*, Journal of materials science letters, 19(17), 1549-1550. (2000).
48. Kim, M. S., Lee, H. T., & Ahn, S. H., *Laser Controlled 65 Micrometer Long Microrobot Made of Ni-Ti Shape Memory Alloy*, Adv. Mater. Technol., 1900583. (2019).

Abstract in Korean

마이크로 로봇의 개발은 기존의 의료 기술을 개선하거나 생명 공학 연구에 새로운 방법을 제공하기 위한 마이크로 기술의 잠재 가치가 있다. 본 연구에서는 형상기억합금 소재의 마이크로 로봇 제작 공정과 제어 방법을 개발하였다. 형상은 집속이온빔 공정으로 제작하였으며, 구성 요소인 구동기가 양방향 형상기억효과를 가지도록 학습하였다. 자외선 레이저를 이용하여 구동하였으며 최대 150.1 μm s^{-1}의 이동속도를 달성하였다. 기본적인 스웜 제어를 구현하기 위해서, 다수의 로봇이 서로 다른 경로로 이동하도록 제어시스템을 구축하였다. 로봇이 레이저 빔의 경로를 따라 움직이도록 제어하여 높은 기동성을 확보하였으며, 목표한 위치로 로봇을 이동시켰다. 마지막으로, 약물을 전달하거나 바늘을 이용한 찌르기와 같은 로봇의 활용 가능성을 제시하였다.

주요어: 스웜, 레이저, 마이크로 로봇, 형상기억합금, 지능재료

학번: 2018-27049